optica

Wide-band slow light in compact photonic crystal coupled-cavity waveguides

Momchil Minkov* and Vincenzo Savona

Laboratory of Theoretical Physics of Nanosystems, Ecole Polytechnique Fédérale de Lausanne (EPFL), CH-1015 Lausanne, Switzerland
**Corresponding author: momchil.minkov@epfl.ch*

Received 28 April 2015; revised 4 June 2015; accepted 8 June 2015 (Doc. ID 239895); published 9 July 2015

Slow light has a variety of applications, in particular for enhanced nonlinear effects like four-wave mixing and high-harmonic generation. Here, we propose a photonic crystal coupled-cavity waveguide with an ultracompact arrangement of the constituent cavities in the propagation direction, and use an optimization algorithm to tune several structural parameters to engineer slow light with a constant group index n_g over a wide bandwidth. We propose several specific silicon designs, including one with $n_g \approx 37$ over a 20 nm wavelength range and another one with $n_g \approx 116$ over an 8.8 nm band, which yields a group index–bandwidth product of 0.66—a record value among all slow-light devices. The design is experimentally beneficial because of its small footprint and straightforward fabrication and could find applications in optical storage or switching, and in generating quantum states of light.

OCIS codes: (230.4555) Coupled resonators; (230.5298) Photonic crystals; (130.5296) Photonic crystal waveguides.

http://dx.doi.org/10.1364/OPTICA.2.000631

One of the major research goals in the field of photonics is enhancing light–matter interactions and the resulting optical nonlinearities. To this end, one approach is to confine light inside an optical cavity for as long as possible—a domain in which silicon photonic crystal (PhC) devices have demonstrated truly outstanding properties [1–4], with quality factors exceeding one million in cavities with modal volumes of the order of the cube of the resonance wavelength in the optical medium. A different approach—better suited for some applications [5]—involves slowing down the light propagation in a one-dimensional structure engineered for a low group velocity where, again, silicon PhCs have led to impressive results [6], particularly in line-defect waveguide systems [7–10] and in coupled-cavity waveguides (CCWs, also called coupled-resonator optical waveguides) [11–17].

There is no unique figure of merit for a slow-light system, but there are several important (and not always independent) parameters. The group index $n_g = c/v_g$, with v_g being the group velocity, is the slow-down factor as compared to the light propagation in vacuum, and nonlinear effects typically scale with this quantity. While it is hard to significantly change the refractive index n of a material using simple manipulations, the group index can be dramatically modified through engineering of the material dispersion since $v_g = d\omega/dk$. In fact, theoretically, n_g can be made arbitrarily large, e.g., in the vicinity of the band edge of a PhC waveguide, but its value is inevitably restricted by effects of localization and light losses due to disorder. Localization (back-scattering) for high n_g in particular has been shown to severely restrict the length scale on which one could meaningfully talk about light transport [18–20]. In practice, the best achieved n_g values are of a few hundred at a given frequency [12,13], with $n_g \approx 100$ in wide-band devices [8]. For a realistic system, it is thus natural to restrict the target n_g values to a similar magnitude, and focus instead on improving other figures of merit. These include low group velocity dispersion (GVD) (i.e., second-order dispersion $d^2\omega/dk^2$), which is necessary for pulsed operation; high delay–bandwidth product (DBP), which, for a fixed group index, means a wide operational bandwidth; and low-loss/high-transmission propagation.

In view of these parameters, PhC CCW systems used thus far have some major pros and cons. The advantages are that a very high n_g with a reasonably low GVD can be achieved, and that losses can be made extremely low using $Q \approx 10^6$ cavities. The disadvantages are that the operational bandwidth is typically small and that having sufficient cavities to obtain a continuous spectrum requires very long (>100 μm) structures, which are very challenging to fabricate. In this Letter, we overcome both of those difficulties in an ultracompact PhC CCW design, which we optimize for a high, constant n_g within a large bandwidth, for several different, experimentally relevant values of the group index.

A few remarks are in order. Following Ref. [21], from here on we use the group index–bandwidth product (GBP, also referred to as the normalized DBP) instead of the DBP as a figure of merit of the CCW performance, and we compute the loss due to out-of-plane radiation in units of [dB/ns] instead of the more standard choice [dB/cm]. This gives the advantage of using quantities which are independent of the device length, and also facilitates the comparison to other systems. In addition, the requirement for low GVD is translated to the related (but not equivalent) requirement [8,21] for an approximately constant n_g: we define a relative variation Δ_R and require $|n_g - \langle n_g \rangle|/\langle n_g \rangle < \Delta_R$. Finally, we remark that for an approximately constant $n_g \approx \langle n_g \rangle$ within a bandwidth $\Delta\omega$, the GBP is $n_g \Delta\omega/\omega \approx \Delta k/\omega$, where Δk is the range of momenta associated to the bandwidth $\Delta\omega$ centered at ω.

Thus, in a periodic structure of period L in the propagation direction, the maximum achievable GBP is given by $\pi/(L\omega)$ and ω is fixed by the target operational wavelength.

Motivated by this consideration, we propose a PhC coupled-cavity array with an extremely short spatial periodicity [Fig. 1(a)]. The structure is based on a triangular lattice of pitch a of air holes of radius $R = 0.25a$ in a silicon ($n = 3.46$) slab of thickness $d = 0.55a$, where the CCW building blocks are L3 cavities, each formed by three missing holes along the x direction [22]. With this particular zigzag arrangement, the unit cell size in the propagation direction y is $2\sqrt{3}a$ but in fact, due to the symmetry with respect to the $x = 0$ axis, the effective periodicity is half this pitch, $L_y = \sqrt{3}a$. Intuitively, this is to say that no gap can open at the boundary of the first Brillouin zone [at $\pi/(2L_y)$], and a larger k space of twice the width can be considered. This is illustrated within a tight-binding approximation in Fig. 1(b) (the mathematical details can be found in Supplement 1). The first- and second-neighbor couplings t_1 and t_2 are identical for the cavities on the left and right of the $x = 0$ plane, and the dispersion curves computed with periodicity L_y (one cavity in the unit cell) or $2L_y$ (two cavities in the unit cell) are plotted for comparison.

For dispersion optimization, we would like to be able to tune the cavity couplings. To a first approximation, we can imagine that modifying the radius of the red and green holes in Fig. 1(a) can be used to control t_1 and t_2, respectively. We see from Fig. 1(b) that when t_2 becomes comparable to t_1, a degeneracy appears within a finite frequency domain which prevents low-GVD propagation. To verify that this can be avoided in our design, in Fig. 2 we show the results of a simulation of a system with two cavities only, arranged in each of the two possible ways as shown in the top insets of each panel. The simulation was performed by solving the full Maxwell equations of the system by employing a guided-mode

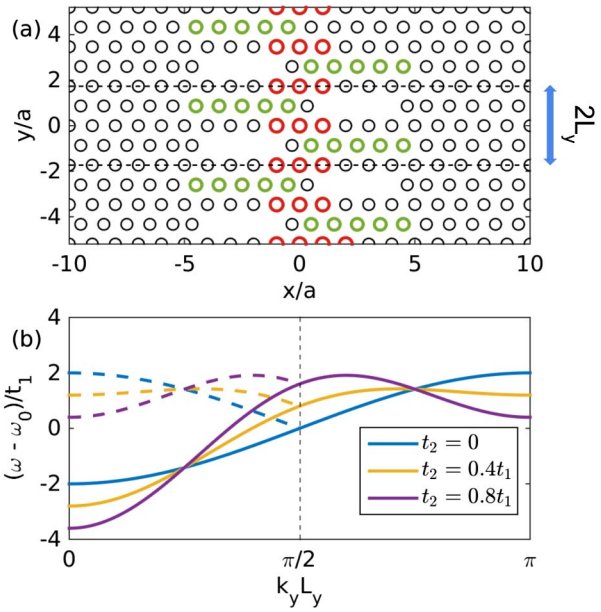

Fig. 1. (a) CCW composed of coupled L3 PhC cavities; the propagation direction is the vertical, y axis. The unit cell of the infinite structure is marked by dashed lines. For dispersion optimization, the radius of all holes marked in red is varied by an amount Δr_1, and that of all holes marked in green by Δr_2. (b) Tight-binding dispersion of a chain of cavities with first- and second-neighbor coupling, t_1 and t_2. The dashed lines show the folded bands in the case of two cavities included in the unit cell, which is an equivalent representation.

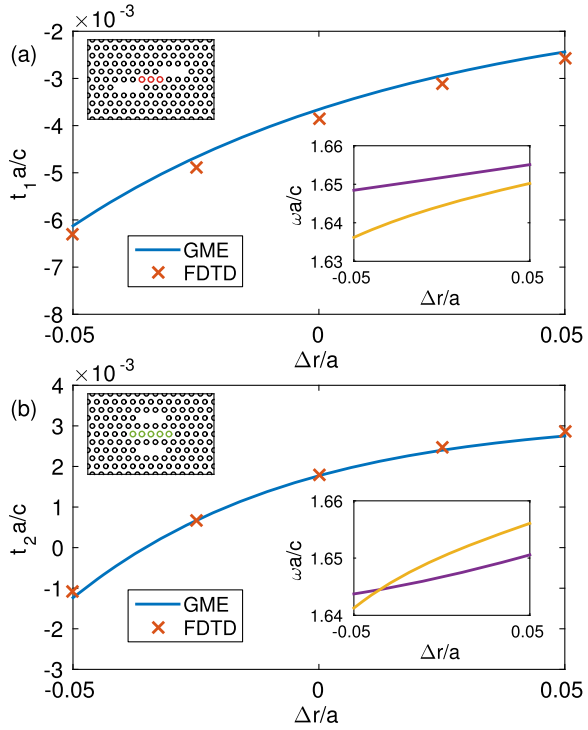

Fig. 2. (a) Cavity–cavity coupling in a system of two cavities arranged as shown in the top inset, depending on the radius change Δr of the holes marked in red. Values obtained with the GME (blue line) and the FDTD (red crosses) methods are shown. Bottom right inset, frequency of the symmetric (yellow) and antisymmetric (purple) modes versus Δr. (b) Same as (a) but for a different arrangement, shown in the top left inset.

expansion method (GME) [23], and also verified with a commercial-grade simulator based on the finite-difference time-domain (FDTD) method [24]. The fundamental modes of the cavities are coupled, producing antisymmetric and symmetric modes, and the splitting $\Delta\omega = \omega_S - \omega_{AS}$ is twice the coupling constant t (see Supplement 1). Thus, t_1 and t_2 can be computed as a function of the radius of the modified holes, and are plotted in Fig. 2. An interesting observation was recently made [25] that in PhCs, the frequency splitting can be either positive or negative, and moreover could be tuned from one sign to the other—crossing zero—by a simple modulation, which we also observe in Fig. 2(b). This is in fact crucial for the compactness of our design, since it allows us to arrange the cavities as shown in Fig. 1(a)—with second neighbors separated by a small physical distance—and still have an arbitrarily small t_2 which, as can be seen in Fig. 2(b), crosses 0 for a given radius change. To conclude this discussion, we note that the tight-binding approximation provides important insights but is rather crude and so, for all simulations below, we use GME to find the true PhC eigenmodes.

Encouraged by these results, we proceed with an optimization of the GBP, using a genetic algorithm to find the optimal PhC parameters in the same manner that has already been successfully applied to the problem of PhC cavity Q optimization [3,4,26]. The GME method is particularly well-suited for dispersion computations as it is an expansion on the basis of propagating modes, and as it assumes periodic boundary conditions. We note that the GME has also proven highly accurate for the computation of out-of-plane losses when compared to first-principle simulations [26,27]. This is important, since the basic L3 cavity has a modest

quality factor of a few thousand [22,23], but this can be increased by several orders of magnitude using some simple modifications of the neighboring holes [26]. Thus, to include the possibility for minimizing losses in the optimization, we allow for a change of radius Δr_3 and an outward shift Δx of the holes on each side of each cavity [marked in white in Fig. 3(a)]. Our free parameters are thus $(\Delta r_1, \Delta r_2, \Delta r_3, \Delta x)$, but we still have freedom in defining the objective function.

We demonstrate several optimizations below to highlight the flexibility of our method. For all computations, we take the standard choice [21] for the maximum allowed relative variation of the group index, $\Delta_R = 10\%$, i.e., we consider the operational bandwidth $\Delta\omega$ to be the one within which $|n_g - \langle n_g\rangle|/\langle n_g\rangle < \Delta_R$ for some value of $\langle n_g\rangle$ (not necessarily the arithmetic average). Thus, after computing $n_g(\omega)$ for a given design, we define the GBP as $G = \langle n_g\rangle \Delta\omega/\omega$, where $\langle n_g\rangle$ is defined such that $\Delta\omega$ is largest. To also account for the radiative losses L_r, the objective function for the design shown in Fig. 3 was set to $f(\Delta r_1, \Delta r_2, \Delta r_3, \Delta x) = G$ for $\max(L_r) < 50$ dB/ns, and to $G \times (50 \text{ dB/ns}/\max(L_r))$ otherwise. The cutoff in the maximum allowed losses was chosen based on the experimentally demonstrated loss in PhC waveguide systems [21].

With this objective function, the optimization results in a design with parameters $(\Delta r_1, \Delta r_2, \Delta r_3, \Delta x) = (-0.0385, -0.0279, -0.0759, 0.1642)a$ [Fig. 3(a)]. The wavelength dispersion plotted in Fig. 3(b) is obtained by setting $a = 400$ nm; as can be seen, the CCW guided band has very low GVD within a very wide wavelength range of 19.5 nm. The average group index is $\langle n_g\rangle = 37$, which results in a GBP of 0.47. This value is more than twice higher than that of previous CCW systems [12,13] and is close to the highest theoretical value of any existing proposal. In fact, the only system to our knowledge which has a higher theoretical GBP is a topology-optimized PhC waveguide [28] with a GBP of 0.5 at $n_g = 50$, which has the significant disadvantage of requiring noncircular holes with fine features that are challenging to fabricate. In another proposal using a coupled-waveguide system [29], the group index and so the GBP vary spatially along the device. A position-averaged GBP value attaining a maximum of approximately 0.5 was estimated for such a system, but the spatial dependence of n_g remains a significant disadvantage as compared to our design.

In order to look for a higher group index n_g, we perform another optimization but aiming at a smaller first-neighbor coupling which, intuitively, results in a smaller frequency width of the guided bands and thus slower light. Practically, we impose this by increasing the distance in the x direction [refer to Fig. 1(a)] between consecutive cavities by one lattice constant a, as illustrated in the inset of Fig. 4(a). Notice that this results in four holes marked in red (radii changed by Δr_1) between consecutive cavities instead of three. Running an optimization with the same objective function as above results in a design with parameters $(\Delta r_1, \Delta r_2, \Delta r_3, \Delta x) = (-0.0049, -0.0340, -0.1016, 0.2204)a$, with $\langle n_g\rangle = 116$ within an 8.8 nm band, thus with a GBP of 0.66 [Figs. 4(a)–4(c)]. This is the highest theoretical GBP among all existing slow-light designs.

Finally, we also obtain designs with an intermediate group index by optimizing each of the two basic designs with a different objective function, defined as $G \times (|\langle n_g\rangle - n_{g,t}|/n_{g,t})$, for some target $n_{g,t}$ (notice that we drop the loss-dependence of the objective function). Setting $n_{g,t} = 80$ results in the design shown in Figs. 4(d)–4(f), with parameters $(\Delta r_1, \Delta r_2, \Delta r_3, \Delta x) = (-0.0208, -0.0350, -0.0950, 0.2443)a$, with $\langle n_g\rangle = 88$ over a 9.9 nm wavelength range (GBP = 0.56). Setting $n_{g,t} = 50$ yields a better design if the three-red-hole scheme of Fig. 3(a) is used; the optimal design [Fig. 4(h) inset] is found for $(\Delta r_1, \Delta r_2,$

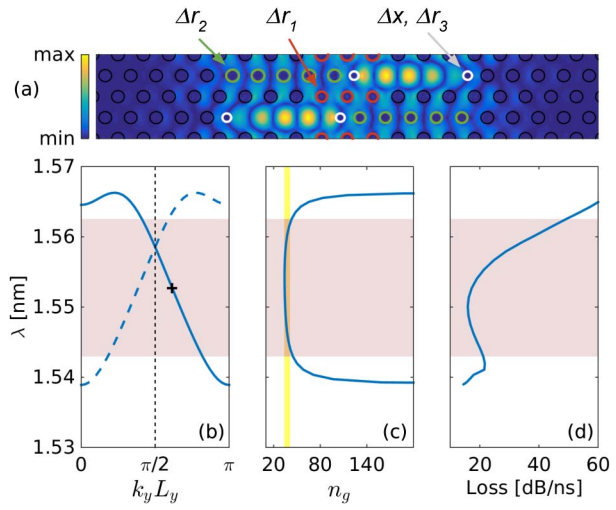

Fig. 3. (a) Electric field $|E_y|$ profile of the mode marked by a black cross in (b). The green and red holes are modified as in Fig. 1(a), while the white holes are shifted outward by an amount Δx and have a radius changed by Δr_3. (b) Wavelength dispersion of the optimized design; the black dashed line marks the Brillouin zone for periodicity $2L_y$. Modes from the dashed-line band propagate in the direction opposite to the one of the solid-line band. The operational bandwidth $\Delta\omega$ is marked by a light red region [extending into panels (c) and (d)]. (c) Group index dispersion; in light yellow, the region $\langle n_g\rangle(1 \pm \Delta_R)$ is marked. (d) Dispersion of the radiative losses.

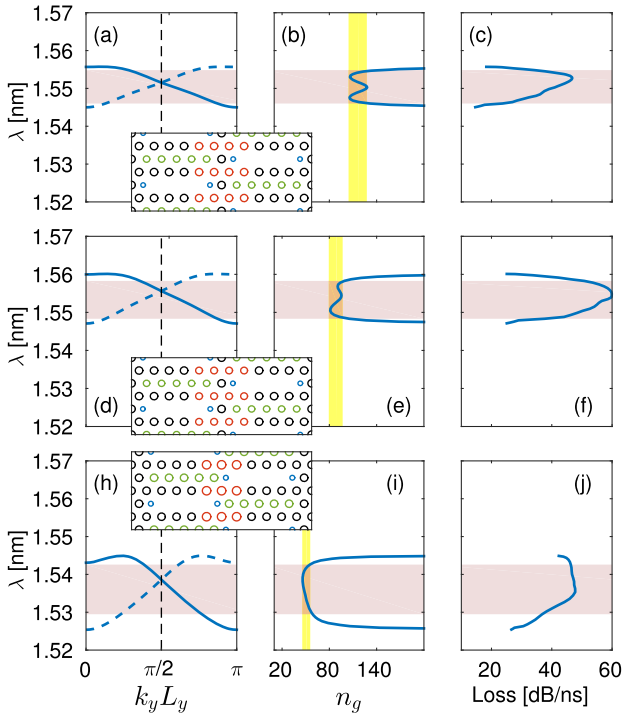

Fig. 4. Designs with (a)–(c) $\langle n_g\rangle = 116$, $G = 0.66$; (d)–(f) $\langle n_g\rangle = 88$, $G = 0.56$; (h)–(j) $\langle n_g\rangle = 51$, $G = 0.43$. The same plotting and color scheme is employed as in Figs. 3(b)–3(d).

$\Delta r_3, \Delta x) = (0.0323, -0.0002, -0.0877, 0.2131)a$, with $\langle n_g \rangle = 51$ over a 13.1 nm bandwidth (GBP = 0.43).

The parameters and figures of merit of all designs are summarized in Table S1 in Supplement 1. There, we also analyze the effect of small deviations of the four parameters ($\Delta r_1, \Delta r_2, \Delta r_3, \Delta x$) from their optimal values. For a deviation of ± 2 nm—larger than the state-of-the-art precision in silicon photonic crystals—we find no degradation of the important figures of merit of the designs, illustrating their practical applicability. Of course, as discussed previously, random disorder in all holes of the structure introduces unavoidable losses both in the vertical and in the counterpropagating direction [18–20], but this was the reason for which we aimed for values of the group index and the extrinsic losses which have been observed in practice in similar systems [8,12]. Finally, we checked that small variations of the material refractive index also preserve the outstanding properties of the proposed designs, and thus they can also be implemented in materials of similar permittivity as silicon, e.g., gallium arsenide.

In conclusion, we present highly optimized designs for silicon coupled-cavity waveguides with a record-high group index–bandwidth product, low variation of the group index, and low out-of-plane losses. The waveguides are straightforward to fabricate and can be used in a variety of applications, including high-bit-rate optical storage (very short pulses can be used due to the large bandwidth) [6,16], enhanced nonlinear effects like four-wave mixing (e.g., for entangled photon pair generation) [10,17,30] and third-harmonic generation [9,31], and enhanced radiative coupling between distant quantum dots for quantum information processing [32,33].

Funding. Schweizerische Nationalfonds zur Förderung der Wissenschaftlichen Forschung (Schweizerische Nationalfonds) (200020_149537).

See Supplement 1 for supporting content.

REFERENCES

1. B. Song, S. Noda, T. Asano, and Y. Akahane, Nat. Mater. **4**, 207 (2005).
2. T. Tanabe, M. Notomi, E. Kuramochi, A. Shinya, and H. Taniyama, Nat. Photonics **1**, 49 (2007).
3. Y. Lai, S. Pirotta, G. Urbinati, D. Gerace, M. Minkov, V. Savona, A. Badolato, and M. Galli, Appl. Phys. Lett. **104**, 241101 (2014).
4. U. P. Dharanipathy, M. Minkov, M. Tonin, V. Savona, and R. Houdré, Appl. Phys. Lett. **105**, 101101 (2014).
5. T. F. Krauss, Nat. Photonics **2**, 448 (2008).
6. T. Baba, Nat. Photonics **2**, 465 (2008).
7. Y. A. Vlasov, M. O'Boyle, H. F. Hamann, and S. J. McNab, Nature **438**, 65 (2005).
8. J. Li, T. P. White, L. O'Faolain, A. Gomez-Iglesias, and T. F. Krauss, Opt. Express **16**, 6227 (2008).
9. B. Corcoran, C. Monat, C. Grillet, D. J. Moss, B. J. Eggleton, T. P. White, L. O'Faolain, and T. F. Krauss, Nat. Photonics **3**, 206 (2009).
10. C. Monat, M. Ebnali-Heidari, C. Grillet, B. Corcoran, B. J. Eggleton, T. P. White, L. O'Faolain, J. Li, and T. F. Krauss, Opt. Express **18**, 22915 (2010).
11. D. O'Brien, M. D. Settle, T. Karle, A. Michaeli, M. Salib, and T. F. Krauss, Opt. Express **15**, 1228 (2007).
12. M. Notomi, E. Kuramochi, and T. Tanabe, Nat. Photonics **2**, 741 (2008).
13. J. Jágerská, N. Le Thomas, V. Zabelin, R. Houdré, W. Bogaerts, P. Dumon, and R. Baets, Opt. Lett. **34**, 359 (2009).
14. J. Jágerská, H. Zhang, N. Le Thomas, and R. Houdré, Appl. Phys. Lett. **95**, 111105 (2009).
15. N. Matsuda, T. Kato, K. Harada, H. Takesue, E. Kuramochi, H. Taniyama, and M. Notomi, Opt. Express **19**, 19861 (2011).
16. H. Takesue, N. Matsuda, E. Kuramochi, W. J. Munro, and M. Notomi, Nat. Commun. **4**, 2725 (2013).
17. H. Takesue, N. Matsuda, E. Kuramochi, and M. Notomi, Sci. Rep. **4**, 3913 (2014).
18. E. Kuramochi, M. Notomi, S. Hughes, A. Shinya, T. Watanabe, and L. Ramunno, Phys. Rev. B **72**, 2 (2005).
19. M. Patterson, S. Hughes, S. Combrié, N. V. Q. Tran, A. Rossi, R. De Gabet, and Y. Jaouën, Phys. Rev. Lett. **102**, 1 (2009).
20. S. Mazoyer, J. P. Hugonin, and P. Lalanne, Phys. Rev. Lett. **103**, 063903 (2009).
21. S. A. Schulz, L. O'Faolain, D. M. Beggs, T. P. White, A. Melloni, and T. F. Krauss, J. Opt. **12**, 104004 (2010).
22. Y. Akahane, T. Asano, B. Song, and S. Noda, Nature **425**, 944 (2003).
23. L. C. Andreani and D. Gerace, Phys. Rev. B **73**, 235114 (2006).
24. Lumerical Solutions, Inc., https://www.lumerical.com/tcad-products/fdtd/.
25. S. Haddadi, P. Hamel, G. Beaudoin, I. Sagnes, C. Sauvan, P. Lalanne, J. A. Levenson, and A. M. Yacomotti, Opt. Express **22**, 12359 (2014).
26. M. Minkov and V. Savona, Sci. Rep. **4**, 5124 (2014).
27. M. Minkov, U. P. Dharanipathy, R. Houdré, and V. Savona, Opt. Express **21**, 28233 (2013).
28. F. Wang, J. S. Jensen, J. Mørk, and O. Sigmund, J. Opt. Soc. Am. A **29**, 2657 (2012).
29. D. Mori and T. Baba, Opt. Express **13**, 9398 (2005).
30. S. Azzini, D. Grassani, M. J. Strain, M. Sorel, L. G. Helt, J. E. Sipe, M. Liscidini, M. Galli, and D. Bajoni, Opt. Express **20**, 23100 (2012).
31. M. Galli, D. Gerace, K. Welna, T. F. Krauss, L. O'Faolain, G. Guizzetti, and L. C. Andreani, Opt. Express **18**, 26613 (2010).
32. S. Hughes, Phys. Rev. Lett. **98**, 083603 (2007).
33. M. Minkov and V. Savona, Phys. Rev. B **87**, 125306 (2013).